Atmos. Chem. Phys. Discuss., 14, 4149–4187, 2014
www.atmos-chem-phys-discuss.net/14/4149/2014/
doi:10.5194/acpd-14-4149-2014


Atmospheric Chemistry and Physics Discussions



# Evolution of the complex refractive index in the near UV spectral region in ageing secondary organic aerosol

**J. M. Flores[1], D. F. Zhao[2], L. Segev[1], P. Schlag[2], A. Kiendler-Scharr[2], H. Fuchs[2], Å. K. Watne[3], N. Bluvshtein[1], Th. F. Mentel[2], M. Hallquist[3], and Y. Rudich[1]**

[1]Weizmann Institute of Science, Department of Earth and Planetary Sciences, Rehovot 76100, Israel
[2]Institut für Energie und Klimaforschung: Troposphäre (IEK-8), Forschungszentrum Jülich, 52425 Jülich, Germany
[3]Dept. of Chemistry and Molecular Biology, Atmospheric Science, University of Gothenburg, 41296 Gothenburg, Sweden

Received: 14 January 2014 – Accepted: 5 February 2014 – Published: 14 February 2014

Correspondence to: Y. Rudich (yinon.rudich@weizmann.ac.il)

Published by Copernicus Publications on behalf of the European Geosciences Union.







## Abstract

The chemical and physical properties of secondary organic aerosol (SOA) formed by the photochemical degradation of biogenic and anthropogenic volatile organic compounds (VOC) are yet poorly constrained. The evolution of the complex refractive index (RI) of SOA, formed from purely biogenic VOC and mixtures of biogenic and anthropogenic VOC was studied over a diurnal cycle in the SAPHIR photochemical outdoor chamber in Jülich, Germany. The correlation of RI with SOA chemical and physical properties such as oxidation level and volatility was examined. The RI was retrieved by a newly developed broadband cavity enhanced spectrometer for aerosol optical extinction measurements in the near UV spectral region (360 to 420 nm). Chemical composition and volatility of the particles were monitored by a high resolution time of flight aerosol mass spectrometer, and a volatility tandem differential mobility analyzer. SOA was formed by ozonolysis of either (i) a mixture of biogenic VOC ($\alpha$-pinene and limonene), (ii) biogenic VOC mixture with subsequent addition of an anthropogenic VOC (p-xylene-$d_{10}$), or (iii) a mixture of biogenic and anthropogenic VOC. The SOA aged by ozone / OH reactions up to 29.5 h was found to be non-absorbing in all cases. The SOA with p-xylene-$d_{10}$ showed an increase of the scattering component of the RI correlated with an increase of the O / C ratio and with an increase in the SOA density. There was a greater increase in the scattering component of the RI when the SOA was produced from the mixture of biogenic VOCs and anthropogenic VOC than from the sequential addition of the VOCs after the approximate same ageing time. The increase of the scattering component was inversely correlated with the SOA volatility. Two RI retrievals determined for the pure biogenic SOA showed a constant RI for up to 5 h of ageing. Mass spectral characterization shows the three types of the SOA formed in this study have significant amount of semivolatile components. The influence of anthropogenic VOCs on the oxygenated organic aerosol, and the atmospheric implications are discussed.





ACPD
14, 4149–4187, 2014



## 1 Introduction

The interaction between aerosols and incoming solar radiation plays an important role in the radiative balance of Earth's atmosphere. Aerosols containing light-absorbing carbonaceous species are a major contributor to the direct and indirect effects on the climate system (Koren et al., 2008; Andreae and Ramanathan, 2013; Bond et al., 2013). Black carbon, which is the dominant absorber of solar radiation in the atmosphere, has fairly well defined optical properties with an estimate of the industrial-era mean direct radiative forcing of approximately $+1.1\,\mathrm{W\,m^{-2}}$ (Bond et al., 2013). However, the optical properties of light-absorbing organic particles, or "brown" carbon (Andreae and Gelencsér, 2006), which may account for 10–40 % of the total light absorption in the atmosphere, and on snow and ice (Park et al., 2010; Bahadur et al., 2012; Cappa et al., 2012; Chung et al., 2012; Kirchstetter and Thatcher, 2012; Feng et al., 2013; Bond et al., 2013), are still poorly constrained. Recent studies estimate the global radiative forcing of brown carbon to be $0.10–0.25\,\mathrm{W\,m^{-2}}$, with higher values on regional scales (Bond et al., 2013; Feng et al., 2013). Brown carbon is mainly produced by combustion sources, especially biomass burning, but it was hypothesized that it can also be produced by atmospheric chemical reactions; for example in the formation of secondary organic aerosols (SOA). SOA can account for 71 % of the total organic aerosol (OA) sources, and up to 85 % when ageing of primary to secondary OA is included (Spracklen et al., 2011). It is presumed that as SOA ages in the atmosphere, high molecular weight compounds can form, subsequently enhancing light absorption. For example, Lambe et al. (2013) showed that the mass absorption coefficient (MAC) at $\lambda = 405\,\mathrm{nm}$ of SOA from biogenic and anthropogenic sources oxidized with OH, increases with increasing oxidation level, but has an overall negligible absorption at $\lambda = 532\,\mathrm{nm}$.

It is important to understand the production of SOA from atmospheric oxidation of biogenic and anthropogenic volatile organic compounds (VOC). Estimations suggest that globally SOA is dominated by biogenic VOC precursors (BVOC), resulting in 90 %





ACPD
14, 4149–4187, 2014



biogenic SOA (BSOA) and 10 % anthropogenic SOA (ASOA) (Hallquist et al., 2009). However, in many case studies, observations of SOA can only be explained assuming enhancement of SOA production by anthropogenic influences (Spracklen et al., 2011). Several studies have shown that the interaction between biogenic volatile organic compounds and anthropogenic VOCs (AVOCs) can significantly affect the properties of SOA (Kautzman et al., 2010; Glasius et al., 2011; Hoyle et al., 2011; Spracklen et al., 2011; Emanuelsson et al., 2013a). Two recent studies have shed some light on the chemical behavior of AVOCs and BVOCs. Hildebrandt et al. (2011) studied the mass yields of SOA formed from mixtures of biogenic and anthropogenic precursors and found that the yields can be parameterized by assuming a common organic phase for partitioning, and that the SOA derived from mixtures of AVOC and BVOC (ABSOA) can be treated as an ideal mixture. Similarly, Emanuelsson et al. (2013a) found that the SOA yields and oxidation levels can be described as linear combinations of the corresponding properties of the pure biogenic and anthropogenic systems.

The complex refractive index (RI; $m = n + ik$) is one of the intrinsic optical properties of aerosols. The real ($n$) and imaginary ($k$) parts express the extent of scattering and absorption of light by the aerosol, respectively. Several studies retrieved SOA refractive indices in the laboratory (Schnaiter et al., 2003; Yu et al., 2008; Wex et al., 2009; Kim et al., 2010, 2012; Lang-Yona et al., 2010; Nakayama et al., 2010, 2012, 2013; Redmond and Thompson, 2011; Lambe et al., 2013; Kim and Paulson, 2013); however, recent studies exploring the evolution of the optical properties of SOA formed from mixtures of AVOCs and BVOCs are not available in the literature. Recently, it became possible to retrieve the RI of aerosols as a function of wavelength using broadband cavity enhanced spectroscopy (Washenfelder et al., 2013; Wilson et al., 2013; Zhao et al., 2013). In this paper we report the evolution of the complex refractive index in the near UV spectral region of ABSOA formed from mixtures of biogenic (a mixture of $\alpha$-pinene and limonene) and anthropogenic (p-xylene-$d_{10}$) precursors at low $NO_x$ levels, by using the approach described in Washenfelder et al. (2013). Additionally, we explore the relationship between the SOA oxidation level, H/C ratio and volatility with





ACPD
14, 4149–4187, 2014



the RI, by following the SOA aging process due to OH oxidation reactions in the outdoor atmospheric simulation chamber SAPHIR over a diurnal cycle.

## 2 Experiments, instrumentation, and methods

### 2.1 Experiments

The experiments took place in the outdoor atmospheric simulation chamber SAPHIR at the Forschungszentrum Jülich, in Jülich, Germany. The SAPHIR chamber has been previously described in detail (Bohn et al., 2005; Rohrer et al., 2005); only a short description will be given here. SAPHIR is a double-walled Teflon chamber with a volume of 270 $m^3$. It is operated with synthetic air (Linde Lipur, purity 99.9999 %), and kept at a slight overpressure of about 50 Pa. To maintain the overpressure in the chamber and to compensate for the sampling by the instruments, a continuous flow of 7–9 $m^3 h^{-1}$ of synthetic air is maintained throughout the experiments. A fan is used to ensure mixing of the injected trace gases, and the chamber is equipped with a Louvre system to either open and expose it to natural sun light or close it to simulate night time processes.

To measure the evolution of the generated SOA, the experiments were performed as follows: after the chamber was flushed throughout the night, synthetic air with about 40 ppm of $CO_2$ was injected into the chamber and the relative humidity was increased to ~ 75 %. Then the chosen VOCs were introduced and allowed to mix for approximately 2 h, followed by injection of 200 ppb of ozone and opening the roof, which marks the beginning of the experiment. The SOA was allowed to age for at least 29 h and only at the end of the experiment the roof was closed. This allowed simulation of a diurnal cycle through which the aerosols aged. Three experiments were performed in this study: (1) a mixture of biogenic VOCs, 48 ppb of $\alpha$-pinene (Sigma-Aldrich, 80605-1ML, ≥ 98.5 %; St. Louis, MO, USA) and 48 ppb of limonene (Sigma-Aldrich, 62 118, ≥ 99 %) were added as precursors with an initial OH concentration of $7.4 \times 10^6$ $cm^{-3}$, referred to as the BVOC experiment; (2) a sequential addition to the BVOC mixture of 39 ppb





ACPD
14, 4149–4187, 2014



of $\alpha$-pinene and 39 ppb of limonene followed by 51 ppb of p-xylene-$d_{10}$ (Sigma-Aldrich, 175927-5G, 99 atom % D) added 5 h after the BVOCs, with an initial OH concentration of $7.8 \times 10^6$ cm$^{-3}$, referred to as the sequential experiment; and (3) a mixture of 42 ppb of $\alpha$-pinene, 42 ppb of limonene, and 90 ppb of p-xylene-$d_{10}$ were added as precursors with an OH concentration of $8.0 \times 10^6$ cm$^{-3}$, referred to as the mixture experiment. The three experiments performed are summarized in Table 1, and Fig. 1 shows a schematic of the experimental procedure.

### 2.2 Analytical instrumentation

The SAPHIR chamber was equipped with temperature, water content, $O_3$, NO, and $NO_2$ monitors. NO and $NO_2$ measurements were performed with a chemiluminescence analyzer (Eco Physics AG, TR480, Duerten, Switzerland) equipped with a photolytic converter (Eco Physics AG, PLC760). Ozone was measured by a UV absorption spectrometer (ANSYCO GmbH, Model O341M, Karlsruhe, Germany). The detection limit and accuracy were 0.5 ppbv and 5 %, respectively. Hydroxyl radical (OH) concentrations were measured using Laser induced fluorescence (LIF). The uncertainty of the OH measurement, determined by the accuracy of the calibration of the LIF instrument, is 10 % ($1\sigma$). The LIF instrument is described in detail by Fuchs et al. (2012). The OH radicals in these experiments are predominantly formed from the ozonolysis of the VOCs, and to a minor extent by HONO and ozone photolysis (Rohrer et al., 2005). The absolute water content was measured with a cavity ring down Picarro analyzer (Picarro G2380, Santa Clara, CA, USA), and was used to calculate the relative humidity. A spectral radiometer (Bohn et al., 2005) was used to measure the actinic flux, the VOCs' concentrations were monitored by a PTR-MS (Jordan et al., 2009), and the total particle concentration and number size distributions were measured by a condensation particle counter (UWCPC, Model 3786, TSI Inc., Shoreview, MN, USA) and a scanning mobility particle sizer (SMPS, TSI 3081 and TSI 3786). Figure 2 shows the time series for the different chamber variables measured for each of the three experiments. The $NO_x$ data is not shown as it was within or below detection limit for all experiments.





ACPD
14, 4149–4187, 2014



## 2.3 Measurement of SOA chemical composition

The chemical composition of the SOA was measured with a High-Resolution Time-of-Flight Aerosol Mass Spectrometer (HR-ToF-AMS, Aerodyne Research Inc., Billerica, MA, USA) (DeCarlo et al., 2006) operated alternatingly between the MS and PToF-mode. The MS mode (in which the ion signals are integrated over all particle sizes) was used to determine the SOA composition. The degree of oxidation of the SOA was characterized by deriving the O/C and H/C ratios (Aiken et al., 2007, 2008), and by determining the ratios $f_{44}$ and $f_{43}$ (defined as the fractions of the signal at $m/z$ = 44 and 43 of the total organics measured by the AMS) and applying them as suggested by Ng et al. (2010). The corrections for the errors due to gaseous components preceded the calculation of the O/C ratio, $f_{44}$ and $f_{43}$ according to the generalized method by Allan et al. (2004).

The density ($\rho$) of the particles, assuming that they are spherical, was calculated using Eq. (1) (DeCarlo et al., 2004):

$$\rho = \frac{d_{va}}{d_m}\rho_0 \quad (1)$$

where $d_{va}$ is the vacuum aerodynamic diameter (obtained from the particle time-of-flight measurements from the TOF-AMS), $d_m$ is the mode mobility diameter from the SMPS size distributions, and $\rho_0$ is the standard density. Calculations of the density are only presented up to 15 h after the experiments began, after that time the vacuum aerodynamic diameter determination became less accurate, probably due to low particle concentrations, and consequently the $\rho$ values became unrealistically variable. However, we do not expect the density trends and values to change significantly after this point.





ACPD
14, 4149–4187, 2014



## 2.4 Measurement of SOA volatility

The volatility of the SOA was determined with a Volatility Tandem Differential Mobility Analyzer (VTDMA), see Jonsson et al. (2007) and Salo et al. (2011) for details. The VTDMA consisted of a Differential Mobility Analyzers (DMA, TSI 3081), eight temperature controlled ovens, and an SMPS (TSI 3081, TSI 3022). First, a narrow particle size distribution was chosen with the first DMA, then the size selected aerosol was directed through one of the eight temperature controlled oven units under laminar flow conditions, and finally classified with the SMPS. To prevent re-condensation of evaporated gases, activated charcoal diffusion scrubbers were used at the exit of the ovens. Each heated oven consists of a 50 cm diameter stainless steel tube mounted on an aluminum block with a heating element set independently to temperature values between 298 to $563 \pm 0.1$ K. The sample flow of $0.3\,\mathrm{L\,min^{-1}}$ was switched between the ovens yielding a residence time in the heated part of the oven of 2.8 s. The aerosol volume fraction remaining (VFR) was calculated assuming spherical particles (Ofner et al., 2011) for the range of elevated temperatures. The VFR decreases with increasing temperature and the data was fitted to a sigmoidal function as has been described by Emanuelsson et. al. (2013b). From the sigmoidal fits it is possible to obtain the temperature where 50 % of the particle volume has evaporated, $T_{\mathrm{VFR0.5}}$. $T_{\mathrm{VRF0.5}}$ was determined every two hours for each experiment, for particles with 100 nm diameter for the first six hours, and 200 nm diameter for the remaining time.

## 2.5 Measurement of SOA optical properties

A dual channel Broadband Cavity Enhanced Spectrometer (BBCES) was used to measure the aerosol optical extinction and retrieve the complex refractive indices between 360 and 420 nm (at 0.5 nm resolution). This instrument follows the design described in Washenfelder et al. (2013), and only a brief description and main differences are given here. The BBCES consist of two optical cavities and a CPC (TSI 3575) connected in series. One channel covers the 360–390 nm and the other covers the 390–420 nm





ACPD
14, 4149–4187, 2014



spectral ranges. Incoherent light emitted from two LEDs with center wavelengths of 370.2 (M365L2, Thorlabs, Newton, NJ, USA) and 407.1 nm (M405L2, Thorlabs) is coupled into each optical cavity with two highly reflective plano-concave mirrors (Advanced Thin Films) situated opposite of each other. The light exiting the cavity is coupled into an optical fiber and transmitted to a 164 mm focal length Czerny–Turner spectrometer (Shamrock SR-163, Andor Technology, Belfast, UK) with a cooled CCD array detector (DU920P-BU, Andor Technology). The spectrometer was calibrated by a reference Hg/Ar lamp. The extinction coefficient ($\alpha_{ext}$) of the aerosol is determined from the change in light intensity of the filled cavity relative to a particle-free cavity; taking into account the mirror reflectivity and the Rayleigh scattering of the carrier gas (Washenfelder et al., 2013).

It has been previously shown that by measuring several particle diameters (assuming the composition of each selected diameter to be the same) and fitting a theoretical Mie curve to the measured extinction cross sections at a specific wavelength, the RI of the aerosol can be retrieved (Pettersson et al., 2004; Lack et al., 2006; Abo Riziq et al., 2007; Lang-Yona et al., 2009; Miles et al., 2010; Bluvshtein et al., 2012; Flores et al., 2012; Washenfelder et al., 2013). The aerosol optical cross-section, $\sigma_{ext}$ ($cm^2$), is determined by Eq. (2):

$$\sigma_{ext}(\lambda, D_p, m) = \frac{\alpha_{ext}(\lambda, D_p, m)}{N(D_p)} \quad (2)$$

where $\lambda$ is the wavelength of the incidence light, $D_p$ is the particle mode diameter, $m$ is the complex refractive index, and $N(D_p)$ is the particle number concentration ($cm^{-3}$). Particles were size-selected between 175–300 nm in 25 nm steps (diameters larger than 250 nm could only be selected towards the end of the experiments). To measure the optical cross section of the size selected SOA from the chamber, aerosol from the SAPHIR chamber was sampled at 1360 $cm^3 min^{-1}$, passed through a diffusion dryer (RH < 30 %), size selected with a DMA (TSI 3081) (with a sheath flow of 11.5 $L min^{-1}$), passed through the BBCES, and counted by the CPC. Each size selection measure-





ACPD
14, 4149–4187, 2014



ment is an average of 150 spectra integrated for 0.3 s. The particle concentration was corrected for dilution by the BBCES mirror purge flows (170 $cm^3 min^{-1}$). The measured extinction cross sections were corrected for multiply charged particles using the closest measured size distributions from the SMPS connected directly to the SAPHIR chamber and the Wiedensohler charge distribution parameterization (Wiedensohler, 1988; with subsequent erratum). Size selection measurements were done, if possible, approximately every two hours and in parallel with the thermal characterization using the VTDMA. To retrieve the real and imaginary components of the RI, the retrieval algorithm was limited to search for $n \geq 1$ and $k \geq 0$, their physical boundaries.

### 2.6 Calculation of Radiative impact

The "simple forcing efficiency" (SFE) proposed by Bond and Bergstrom (2006) can be used to estimate changes in direct forcing of the ageing SOA. We use the wavelength-dependent version (Chen and Bond, 2010) to calculate the change in the radiative impact of the aged SOA:

$$\frac{\mathrm{dSFE}}{\mathrm{d}\lambda} = -\frac{1}{4}\frac{\mathrm{d}S(\lambda)}{\mathrm{d}\lambda}\tau_{\mathrm{atm}}^2(\lambda)(1-F_{\mathrm{c}})\left[2(1-a_s)^2\beta(\lambda)\cdot\mathrm{MSC}(\lambda) - 4a_s\cdot\mathrm{MAC}(\lambda)\right] \quad (3)$$

where $\mathrm{d}S(\lambda)/\mathrm{d}\lambda$ is the solar irradiance, $\tau_{\mathrm{atm}}$ is the atmospheric transmission, $F_{\mathrm{c}}$ is the cloud fraction (0.6), $a_{\mathrm{s}}$ is the surface albedo (average of 0.19), $\beta$ is the backscatter fraction, and MSC and MAC are the mass scattering and mass absorption cross sections per gram, respectively. The wavelength-dependent solar irradiance and atmospheric transmission are taken from the ASTM G173-03 Reference Spectra. For this study, the calculation is done from 360 to 950 nm to observe the differences in the visible spectrum. To calculate $\beta(\lambda)$, MSC($\lambda$), and MAC($\lambda$) the retrieved RI from this study is used for the 360–420 nm range, and a constant RI is assumed for larger wavelengths, taking the retrieved RI at $\lambda$ = 420 nm as the value for this spectral region. For the MAC($\lambda$)





ACPD
14, 4149–4187, 2014



calculation, we also use the $\rho$ values calculated by Eqs. (1) and (4):

$$\mathrm{MAC} = \frac{4\pi k}{\rho} \tag{4}$$

## 3 Results

### 3.1 Refractive indices of SOA from pure BVOC and mixtures of BVOC and AVOC

Oxidative ageing can cause changes in the RI of SOA (Liu and Daum, 2008; Cappa et al., 2011; Nakayama et al., 2012, 2013; Lambe et al., 2013), as the chemical speciation, mean molecular weight, density and polarizability of the SOA change with aging. For all retrievals in this study, the imaginary part reached zero at all wavelengths; in other words, there was no detectable absorption under the conditions in this study. Consequently, only the retrieved real part of the RI as a function of wavelength between 360–420 nm for the three different experiments performed are shown in Fig. 3. For clarity, the shown retrieved real parts are averaged every 1.5 nm, the errors for each wavelength were averaged and the average of the errors is shown on the left side of each panel (red symbols), and, for the mixture experiment, only three out of six retrievals are shown.

Figure 3a shows the results for the BVOCs experiment with the ageing induced by OH reactions. Typical $NO_X$ levels were $< 0.3$ ppbv. For comparison, other studies of $\alpha$-pinene SOA ageing by ozone and OH reactions are also included. From Fig. 3a we can see that the real part remains constant within the calculated error range up to 5 h after the experiment began, with $n$ values varying from 1.511 (±0.011) at $\lambda = 360$ nm to 1.485 (±0.010) at $\lambda = 420$ nm. Due to technical problems only two retrievals could be obtained for this experiment. The results of the sequential experiment (p-xylene-$d_{10}$ was added five hours after SOA formation from the $\alpha$-pinene and limonene mixture) are shown in Fig. 3b. For this experiment, the real part increased from a value of $n = 1.500$ (±0.004) to $n = 1.520$ (±0.012) at $\lambda = 360$ nm, and from $n = 1.451$ (±0.003)





ACPD
14, 4149–4187, 2014



to $n = 1.487$ ($\pm 0.022$) at $\lambda = 420$, from the first measurement at 4.5 h to 29 h of ageing. Contrary to the BVOC experiment, there is a clearer increase in the real part. Figure 3c shows the results for the mixture experiment (the $\alpha$-pinene and limonene mixture and p-xylene-$d_{10}$ were added simultaneously). Here there is an increase in the real part of the RI from 1.5 h to 25.2 h of ageing, changing from $n = 1.490$ ($\pm 0.006$) to $n = 1.540$ ($\pm 0.009$) at $\lambda = 360$ nm, and from $n = 1.454$ ($\pm 0.008$) to 1.485 ($\pm 0.017$) at $\lambda = 420$ nm. The three experiments show a slight spectral dependence of the real part of the RI with higher values of the real part at shorter wavelengths.

### 3.2 Refractive indices – literature comparison

In the past few years, several laboratory studies have retrieved the complex refractive indices of SOA generated from biogenic and anthropogenic precursors (Schnaiter et al., 2003; Wex et al., 2009; Kim et al., 2010, 2012; Lang-Yona et al., 2010; Cappa et al., 2011; Nakayama et al., 2012, 2013; Kim and Paulson, 2013; Lambe et al., 2013), with only a few retrieving the RIs in the near UV spectral region. For example, for SOA generated from the ozonolysis of $\alpha$-pinene, Liu et al. (2013) found values of the real part of $n = 1.517$ ($\pm 0.003$) and $n = 1.509$ ($\pm 0.003$) for $\lambda = 360$ nm and $\lambda = 420$ nm, respectively, using a variable angle spectroscopic ellipsometer. The imaginary components they found in this range were below $k < 10^{-4}$. Using cavity ring down spectroscopy (CRDS), Nakayama et al. (2012) retrieved values between $n = 1.463$ ($\pm 0.019$) and $n = 1.475$ ($\pm 0.022$) at $\lambda = 405$ nm, and Nakayama et al. (2010) found values of $n = 1.458$ ($\pm$ 0.019) at $\lambda = 355$ nm. The imaginary parts for both studies were found to be below 0.003. Wex et al. (2009) retrieved only the real part of the RI by using a white light optical particle spectrometer, and found a value of $n = 1.45$ for the visible wavelengths. Similarly, Schnaiter et al. (2003) determined a constant value of $n = 1.44$ for $\lambda > 350$ nm by measuring the wavelength dependence of the SOA scattering and extinction. Using CRDS and a photo-acoustic sensor to measure RIs Lambe et al. (2013) found values between $n = 1.51$ ($\pm 0.02$) and $n = 1.45$ ($\pm 0.04$) with imaginary part values of $k < 0.001$ at $\lambda = 405$ nm for SOA formed by homogeneous nucleation and conden-





ACPD
14, 4149–4187, 2014



sation following OH oxidation of $\alpha$-pinene at different oxidation levels, using a potential aerosol mass flow tube reactor.

For SOA formed by ozonolysis of limonene, we could only find one study that measured the RI in the near UV spectral region. Liu et al. (2013) measured $n$ values between 1.520 (±0.003) and 1.512 (±0.003) and imaginary parts below $k < 10^{-4}$ for wavelengths between 420 and 360 nm. Recently, Kim and Paulson (2013) measured the real part of the RI for SOA generated from the ozonolysis of $\alpha$-pinene and limonene with and without an OH scavenger in a Teflon chamber using a polar nephelometer at $\lambda = 532$ nm. For both SOA products, they found that the real part of the RI increased from 1.39 (±0.03) to 1.52 (±0.03) as the particles sizes grew in time (up to 4 h), with no discernible effect when an OH scavenger was used.

### 3.3 Relationship between oxidation level and refractive index

Oxidative ageing changes the SOA's oxidation state, density, mean molecular weight, and polarizability (Katrib et al., 2005; Liu and Daum, 2008; Cappa et al., 2011; Lambe et al., 2013). O/C and H/C ratios are useful metrics to measure the oxidative state of the aerosol (Ng et al., 2010). Figure 4 shows the change in the retrieved complex refractive index (real part only) for wavelengths between 360–420 nm as a function of the O/C ratio (Fig. 4a1, 4b1 and 4c1), H/C ratio (Fig. 4a2, 4b2 and 4c2), and $T_{VFR0.5}$ (Fig. 4a3, 4b3 and 4c3) as the SOA evolved with time.

It can be seen that for the mixture experiment, the value of the RI increases with SOA ageing. This is correlated with the SOA increasing oxidation level (Fig. 4c1): the O/C values increase from ~ 0.34 at 1.5 h to ~ 0.42 at 29 h of ageing, the H/C ratio decreases (Fig. 4c2) from ~ 1.55 to 1.49, and the volatility (Fig. 4c3) decreases with $T_{VFR0.5}$ increasing from ~ 366 K (±2) up to ~ 388 K (±1). There is a similar trend for the sequential experiment. However, the magnitude of the increase in RI with respect to the O/C ratio is smaller, even though the O/C ratio increased more (~ 0.44) for approximately the same ageing time. Furthermore, the rate of change of the RI with respect to the H/C ratio is also smaller than for the mixture experiment: the H/C ratio





ACPD
14, 4149–4187, 2014



decreased from around 1.50 to ~ 1.45. There is not a clear difference between the two experiments in the dependence of the real part of the RI on volatility. For the BVOCs experiment it is difficult to assess a relationship with only two retrievals within the first 5 h of the experiment. There is only evidence that the RI remained constant (as seen in Fig. 3) with a small increase in the O/C ratio, and a slight decrease in volatility with $T_{VFR0.5}$ increasing from 365.5 K (±2.7) to 366.7 K (± 2.6).

The relationship between optical properties and chemical composition has been previously explored. Table 2 summarizes the different studies that have related the RI to the O/C ratio. Lambe et al. (2013) measured the real part of the RI at $\lambda$ = 405 nm for SOA formed from the OH oxidation of $\alpha$-pinene, naphthalene and tricyclo-decane (anthropogenic surrogate precursors), and guaiacol (biomass burning surrogate precursor). They observed a decrease in $n$ with increase in SOA oxidation level. For $\alpha$-pinene, an O/C = 0.42 at the beginning of the experiment, increasing to an O/C = 0.93, and an RI decrease from $n$ = 1.51 (±0.02) to 1.45 (±0.04) were obtained. They also observed a slight increase in the imaginary component of the RI from $k$ = 0 to 0.001; however, these values are very low. In contrast, Cappa et al. (2011) who studied the heterogeneous OH oxidation of squalane (a saturated hydrocarbon) and azelaic acid (a dicarboxylic acid) particles at $\lambda$ = 532 nm, observed an increasing trend with similar oxidation levels (O/C = 0–0.35) compared with the ones measured in this study. They measured an increase in the real part from about $n$ = 1.47 (± 0.02) at O/C = 0.0 to about $n$ = 1.52 at O/C = 0.35 for squalene, and from $n$ = 1.46 to 1.55 for azelaic acid at O/C ratios from 0.45 to 0.75. Nakayama et al. (2013) also saw an increasing trend studying the RI of SOA generated from the photooxidation of toluene (an aromatic hydrocarbon). At $\lambda$ = 405 nm the real part increased from $n$ = 1.449 (± 0.030) to $n$ = 1.567 (± 0.042), and at $\lambda$ = 532 nm from $n$ = 1.431 (±0.026) to $n$ = 1.498 (±0.025) for O/C values from 0.64 to 0.73. Nakayama et al. (2012) retrieved RI values for SOA produced from the ozonolysis and photooxidation of $\alpha$-pinene, and found values from $n$ = 1.463 (±0.019) to $n$ = 1.475 (±0.022) at $\lambda$ = 405 nm and $n$ = 1.476 (± 0.021)–1.458 (± 0.020)





ACPD
14, 4149–4187, 2014



at $\lambda = 532$ nm for O/C ratios from 0.43 to 0.47. Therefore, it is difficult to assess a decreasing or increasing trend from the Nakayama et al. (2012) study.

### 3.4 Chemical ageing

To help assess the chemical changes in the different SOA and compare them to literature values, Fig. 5 shows a van Krevelen diagram (van Krevelen, 1950) of the H/C ratio as a function of the O/C ratio. Figure 5a shows that the H/C ratio for the BVOC and sequential experiment show a similar behavior, the H/C ratio remains nearly constant for the first few hours of the experiment and then decreases. For the BVOC experiment the H/C ratio starts at around 1.50 and decreases to about 1.40, and in the sequential experiment begins at 1.51 that decreases to ~ 1.43. The mixture experiment, however, shows an increase of the H/C ratio in the first few hours of the experiment, from 1.51 to 1.57, followed by a decrease to ~ 1.49 at the end of the experiment.

In the evolution of the O/C and H/C ratios there are three distinct features: (1) the initial increase in the H/C ratio, especially seen in the mixture experiment; (2) the increase of the O/C ratio during day time with the H/C remaining almost constant; and (3) the O/C remaining constant, even decreasing, during night time while the H/C decreased. The initial increase of the H/C to O/C ratio occurs in the phase of vigorous chemistry and particle growth at the instance ozone is added. There are two overlapping processes occurring in this stage: chemical ageing, which increases the O/C ratio and lowers the H/C ratio (e.g. pinic acid, multiple ketones), and fast growth by dissolution of semivolatile oxidized products, which maintains the O/C ratio of the precursors (e.g. pinonic acid, pinonealdehyde, hydroperoxides), but has an increasing effect on the H/C ratio. The strongest effect in the initial increase of the H/C ratio, with the simultaneous O/C increase, is clearly seen in the mixture experiment. This may be due to the oxidation conditions, or it could reflect the influence of p-xylene-$d_{10}$. The difference is not clear as the three experiments began with similar temperatures, RH values, pressure and OH concentrations (Fig. 2). However, the initial ozone concen-





ACPD
14, 4149–4187, 2014



tration and solar radiation exposure were lower for the mixture experiment than for the other two experiments.

Following this initial stage, the mixtures are photochemical aged, with an OH concentration of about 2–3 × $10^6$ molecules $cm^{-3}$ (see Fig. 2 middle panels) for the three experiments. Here there are slight differences in the O/C values between the BVOC and sequential experiment. This might be caused by either the addition of p-xylene-$d_{10}$ 5 h after the insertion of the $\alpha$-pinene-limonene mixture, or the specific oxidation conditions. However, there were no significant differences between the experimental initial conditions, neither the meteorological condition nor the VOC and $O_3$ concentrations.

During the night the O/C ratio remained constant, showing a slight decrease in the BVOC and sequential experiments, while the H/C ratio decreased. The slight decrease of O/C overnight might be due to reactions in the particulate phase (e.g oligomerization). The observed decrease in the H/C ratio during the night is probably caused by the dilution flow into the chamber which depletes the gas phase, including semivolatile oxidized compounds, leading to their evaporation. The excess of semivolatiles, caused by the high initial load of monoterpenes ceases at the end of the night and onset of the next day. This is seen by the simultaneous decrease of H/C and O/C; at this stage the molecules were converted to higher oxidized generations by OH reactions during the second day.

## 4 Discussion

By comparing the H/C and O/C ratios measured in this study to values measured in different cities around the world (Fig. 5b), it is clear that the SOA in this study is less oxidized. The fact that the SOA is not as oxidized may explain the lack of absorption observed, though Nakayama et al. (2012) measured similar values of the H/C and O/C ratios and also found negligible absorption. Cappa et al. (2011) with higher values of the H/C ratio and lower values of the O/C ratio assumed purely scattering particles. Lambe et al. (2013) which were able to age BSOA formed from OH oxidation of $\alpha$-





ACPD
14, 4149–4187, 2014



pinene (Fig. 5b, red triangles) up to an O/C = 0.93 and an H/C = 1.1 only saw an increase in the imaginary component from $k = 0$ to $k = 0.001$. And for ASOA, formed from the OH oxidation of naphthalene, they saw an increase in k up to 0.0035 for an O/C = 1.3 and H/C = 0.84. Only Nakayama et al. (2013) saw slightly higher absorption at O/C ratios between 0.64–0.73, but for SOA generated from the photooxidation of toluene at different $NO_x$ levels, with measured $k$ values between 0.0018 (±0.0014) and 0.0072 (±0.0010) at $\lambda = 405$ nm.

The values of the real part retrieved in this study are within the values reported in the literature; however, there is a significant span in the real part, from $n = 1.44$ to $n = 1.58$, among all the studies (for example, see the values at $\lambda = 405$ nm in Table 2 and Fig. 3). The differences in RI values suggest differences in the SOA chemical composition, which can arise from several different factors; for example, the initial VOC and its concentration, oxidant levels, formation temperature and relative humidity, the residence times in either the flow tubes or chamber experiments, and the experimental procedure. The differences in the SOA chemical composition from different initial VOC concentration (which will directly influence the initial mass concentration) seems unlikely; on the one hand, Bateman et al. (2011) and Walser et al. (2008) demonstrated that the composition of limonene + $O_3$ SOA formed in either a smog chamber with low mixing ratios (< 0.1 ppmv) or a flow tube with significantly higher (~ 10 ppmv) mixing ratios, is similar. On the other hand, Shilling et al. (2009) saw small composition differences of $\alpha$-pinene SOA when mass concentrations were above 20 $\mu g\,m^{-3}$. All the studies reported here used mass concentration greater than 20 $\mu g\,m^{-3}$; hence, no significant differences in the RIs would be expected. The oxidation level may perhaps explain the differences; however, there are no clear trends from the available studies. For example, Lambe et al. (2013) showed that the real part of the RI decreases with increasing oxidation, and Liu et al. (2013) mentioned that the low oxidation level of their SOA (from Shilling et al. (2009) this would correspond to an O/C < 0.3 as the mass loading was > 140 $\mu g\,m^{-3}$) could possibly explain that their measured $n$ values are higher than the other reported values. In contrast, Cappa et al. (2011) and Nakayama





ACPD
14, 4149–4187, 2014



et al. (2013) observed the opposite trend; i.e., an increase in the real part with increasing O/C ratio, which is the same trend observed in this study. The initial increase in the real part of the RI in this study might be explained by the change in the SOA density. One form of the Lorentz–Lorentz relation associates the RI to the mean polarizability ($\alpha$), the molecular weight (MW) and the density of the particle:

$$\frac{(n^2-1)}{(n^2+2)} = \frac{\alpha \cdot \rho}{3 \cdot \mathrm{MW}} \quad (5)$$

Furthermore, Liu and Daum (2008) showed that the real part of the refractive index increases with mass density, and Katrib et al. (2005) showed the density of layers of oleic acid increases as the oxygen content also increases. Figure 6a shows the change in SOA density with time for the three experiments; only values up to 15 h after the experiments began are shown, and Fig. 6b shows the change in RI vs. density. Figure 6b clearly shows the concomitant increase in the real part of the RI and density for the sequential and mixture experiments, while Fig. 6a demonstrates the $\rho$ increase for all experiments and the distinct differences in change of density with time among the three experiments. For example, the BVOC experiment shows the lowest values up until about 14 h after the beginning of the experiment, when it acquires the same values as the sequential experiment, while the mixture experiment shows consistently higher values than the BVOC and sequential experiments. The increase in $\rho$ seen in Fig. 6b can help explain the increase in the real part of the RI seen in the mixture (Fig. 4c1) and sequential experiments (Fig. 4b1), and assuming the trends between the experiments remain the same up to 30 h after the experiments began, the greater increase in the RI in the mixture experiment. Figure 6b also demonstrates the influence of the MW due to the addition of p-xylene-$d_{10}$, as the initial RI for the BVOC experiment is higher than the sequential and mixture experiments.





ACPD
14, 4149–4187, 2014



## 5 Atmospheric relevance and implications

To assess the atmospheric relevance of the SOA measured in this study Fig. 7 shows the $f_{44}$ vs. $f_{43}$ ratio measured for the three experiments presented here. Ng et al. (2010) suggested that the ratio $f_{44}/f_{43}$ can be used to estimate the degree of oxidation and volatility, within the oxygenated organic aerosol (OOA) components; they defined the less oxidized components (lower $f_{44}$) as semi-volatile OOA and the more oxidized (higher $f_{44}$) as low-volatility OOA. In other words, a low $f_{44}/f_{43}$ value can be used as an indication of semi-volatile OOA and a higher $f_{44}/f_{43}$ value indicates lower volatility OOA. The triangle in the insert in Fig. 7 shows the area proposed by Ng et al. (2010) which encompasses the majority of the OOA measured in the field. It can be seen that the SOA studied here fall within the lower right section of the triangle and are overall similar, suggesting that the SOA formed in these experiments may be semi-volatile. Furthermore, Fig. 7 shows that for all three experiments the $f_{44}$ signal increases and $f_{43}$ decreases as the SOA age, from approximately $f_{44} = 0.05$ to $\sim 0.08$ to 0.10 and from $f_{43} = 0.16$ down to $\sim 0.12$, confirming that the SOA became less volatile with time, as shown in Fig. 4b3 and 4c3. Moreover, whereas there is no distinguishable difference in the $f_{44}/f_{43}$ signals between the BVOCs and sequential experiment, the mixture experiment has a lower $f_{43}$ signal at a given $f_{44}$ suggesting that BSOA have less volatile components ($f_{43}$) than ABSOA at the same degree of oxidation ($f_{44}$). It further suggests that the interaction of p-xylene-$d_{10}$ with $\alpha$-pinene and limonene in the mixture experiment can change the chemical and volatility properties of the ABSOA formed in comparison to the properties of BSOA; whereas the interaction of p-xylene-$d_{10}$ with BSOA in the sequential experiment does not significantly alter the chemical and volatility properties. However, overall the mass spectral characteristics do not show enough differences to distinguish the influence of anthropogenic VOCs on the oxygenated organic aerosol. Figure 7 also shows that even though the BSOA and ABSOA were not oxidized significantly and the initial BVOC and AVOC concentrations are higher than atmospherically relevant concentrations, the oxidation and volatility levels of the SOA





ACPD
14, 4149–4187, 2014



fall within an atmospherically relevant range; specifically at the edge of large $f_{43}$, i.e. there is large influence of semivolatiles.

To assess the change in the direct forcing of the ageing SOA we use the simple forcing efficiency in watts per gram (Sect. 2.6, Eq. 3). The SFE is illustrative only (Chen and Bond, 2010) and to determine the actual change in forcing efficiency a climate model has to be used. In order to obtain the maximal change in the forcing efficiency from the data, only the first (1.5 h after the experiment began) and last retrievals (29.25 h after the experiment began) of the mixture experiment are used for the calculation, as it showed the greatest change in the RI. A surface albedo of 0.19 (Earth's average) was used. The Mie simulations assumed a median diameter of 150 nm and 200 nm for the first and last retrievals, respectively, taken from the measured size distributions (see Fig. 2) and, since there was no detectable absorption, a $k = 0.0001$ was used for the calculations. A density of $\rho = 1.37\,\mathrm{g\,cm^{-3}}$ was used for the first retrieval and a $\rho = 1.45\,\mathrm{g\,cm^{-3}}$ for the last. The $n$ values used for $\lambda > 420$ nm are 1.456 and 1.502 for the first and last retrieval, respectively. As a comparative example the SFE was also calculated assuming the imaginary part increased to $k = 0.01$ for the last retrieval.

Figure 8 shows the SFE at each wavelength for the three cases. The integrated forcing over the calculated range is $-24\,\mathrm{W\,g^{-1}}$ for the first retrieval, $-36\,\mathrm{W\,g^{-1}}$ for the last one with $k = 0.0001$, and $-32\,\mathrm{W\,g^{-1}}$ for the assumed example with $k = 0.01$. This indicates that the observed change in refractive index due to ageing, without an increase in absorption, can lead to overall cooling. Furthermore, with an average change in $n$ of $\Delta n = 0.046$ and an increase in the imaginary part of $k = 0.01$ (the maximum change observed in the literature was $k = 0.0072$ ($\pm$ 0.0010) at $\lambda = 405$ nm (Nakayama et al., 2013)), there is still an overall cooling with respect to the initial RI of the SOA.

## 6 Conclusions

We have measured the evolution of the complex refractive index in the near UV spectral region, between 360 and 420 nm, of BSOA and ABSOA formed from three dif-





ACPD
14, 4149–4187, 2014



ferent mixtures of biogenic (a mixture of $\alpha$-pinene and limonene) and anthropogenic (p-xylene-$d_{10}$) VOCs at low $NO_x$ levels. Additionally, we have explored the relationship of the oxidation level, H/C, and volatility with the RI as the SOA ages due to OH oxidation in the outdoor atmospheric simulation chamber SAPHIR over a diurnal cycle. One experiment consisted of pure BSOA produced from a 1 : 1 mixture of $\alpha$-pinene and limonene, the other two experiments consisted of ABSOA, one with the ABSOA produced from the sequential addition of a 1 : 1 mixture of $\alpha$-pinene and limonene followed by p-xylene-$d_{10}$, and the other with the ABSOA produced from a mixture of $\alpha$-pinene, limonene and p-xylene-$d_{10}$. We found an increase in the real part of the RI with ABSOA ageing, and no detectable absorption in any of the experiments. Furthermore, we observed a correlation between the increase in the real part of the RI and the increase of the O/C ratio, with a greater increase in RI when the ABSOA is produced from the mixture of BVOCs and AVOC than from the sequential addition of the VOCs after the approximate same ageing time. This suggests the interaction of BVOCs and AVOCs can make the ABSOA a more scattering aerosol. The increase in the real part points to the fact that it can be associated with an increase in the aerosol density. On the other hand, we only have RI retrievals up to 5 h of ageing for the BSOA and could not assess how much the real part increases, if at all, over a diurnal cycle. We also observed differences in the volatility and the H/C ratio between the BSOA and the ABSOA. From analyzing the $f_{44}$ vs. $f_{43}$ ratios measured for the three experiments, all three types of SOA can be considered semi-volatile oxygenated organic aerosols, and it is suggested that the interaction of AVOC and BVOC can form ABSOA with different chemical and volatility properties than pure BSOA of BSOA that interacts with AVOC. A caveat with respect to generalization of the results obtained in this study is that the SOA measured is less oxidized than SOA measured in different cities around the world. The O/C values in the three experiments ranged from $\sim$ 0.35 to 0.44, whereas the ones measured in the field are between 0.54 and 1.02.





ACPD
14, 4149–4187, 2014



The results from this study demonstrate that the optical properties of SOA are influenced by the interaction of BVOCs and AVOCs, are in continuous evolution, and the magnitude of their change depends explicitly on the formation mechanism of the SOA.

*Acknowledgements.* This study was partially supported by the German-Israeli Foundation for Scientific Research and Development, Research Grant No. 1136-26.8/2011, by the EUROCHAMP2 transnational access activity E2-2012-04-22-0072, and by FP7-ENV-2010-265148-PEGASOS. JMF is supported by a research grant from the Jinich Postdoctoral Fellowship. We thank the SAPHIR team, especially Franz Rohrer, Birger Bohn, Rolf Häseler, Martin Kaminski, Anna Lutz and Ismail-Hakki Acir for providing helpful data and supporting our measurements. We also thank Steve S. Brown and Rebecca Washenfelder for helpful discussions and support with the optical system.

## References

Abo Riziq, A., Erlick, C., Dinar, E., and Rudich, Y.: Optical properties of absorbing and non-absorbing aerosols retrieved by cavity ring down (CRD) spectroscopy, Atmos. Chem. Phys., 7, 1523–1536, doi:10.5194/acp-7-1523-2007, 2007.

Aiken, A. C., DeCarlo, P. F., and Jimenez, J. L.: Elemental analysis of organic species with electron ionization high-resolution mass spectrometry, Anal. Chem., 79, 8350–8358, 2007.

Aiken, A. C., DeCarlo, P. F., Kroll, J. H., Worsnop, D. R., Huffman, J. A., Docherty, K. S., Ulbrich, I. M., Mohr, C., Kimmel, J. R., Sueper, D., Sun, Y., Zhang, Q., Trimborn, A., Northway, M., Ziemann, P. J., Canagaratna, M. R., Onasch, T. B., Alfarra, M. R., Prevot, A. S. H., Dommen, J., Duplissy, J., Metzger, A., Baltensperger, U., and Jimenez, J. L.: O/C and OM/OC ratios of primary, secondary, and ambient organic aerosols with high-resolution time-of-flight aerosol mass spectrometry, Environ. Sci. Technol., 42, 4478–4485, 2008.

Allan, J. D., Delia, A. E., Coe, H., Bower, K. N., Alfarra, M. R., Jimenez, J. L., Middlebrook, A. M., Drewnick, F., Onasch, T. B., Canagaratna, M. R., Jayne, J. T., and Worsnop, D. R.: A generalised method for the extraction of chemically resolved mass spectra from Aerodyne aerosol mass spectrometer data, J. Aerosol Sci., 35, 909–922, 2004.

Andreae, M. O. and Gelencsér, A.: Black carbon or brown carbon? The nature of light-absorbing carbonaceous aerosols, Atmos. Chem. Phys., 6, 3131–3148, doi:10.5194/acp-6-3131-2006, 2006.





ACPD
14, 4149–4187, 2014



Andreae, M. O. and Ramanathan, V.: Climate's dark forcings, Science, 340, 280–281, 2013.
Bahadur, R., Praveen, P. S., Xu, Y., and Ramanathan, V.: Solar absorption by elemental and brown carbon determined from spectral observations, P. Natl. Acad. Sci. USA, 109, 17366–17371, 2012.
Bateman, A. P., Nizkorodov, S. A., Laskin, J., and Laskin, A.: Photolytic processing of secondary organic aerosols dissolved in cloud droplets, Phys. Chem. Chem. Phys., 13, 12199–12212, 2011.
Bluvshtein, N., Flores, J. M., Riziq, A. A., and Rudich, Y.: An approach for faster retrieval of aerosols' complex refractive index using cavity ring-down spectroscopy, Aerosol Sci. Tech., 46, 1140–1150, 2012.
Bohn, B., Rohrer, F., Brauers, T., and Wahner, A.: Actinometric measurements of $NO_2$ photolysis frequencies in the atmosphere simulation chamber SAPHIR, Atmos. Chem. Phys., 5, 493–503, doi:10.5194/acp-5-493-2005, 2005.
Bond, T. C. and Bergstrom, R. W.: Light absorption by carbonaceous particles: an investigative review, Aerosol Sci. Tech., 40, 27–67, 2006
Bond, T. C., Doherty, S. J., Fahey, D. W., Forster, P. M., Berntsen, T., DeAngelo, B. J., Flanner, M. G., Ghan, S., Kärcher, B., Koch, D., Kinne, S., Kondo, Y., Quinn, P. K., Sarofim, M. C., Schultz, M. G., Schulz, M., Venkataraman, C., Zhang, H., Zhang, S., Bellouin, N., Guttikunda, S. K., Hopke, P. K., Jacobson, M. Z., Kaiser, J. W., Klimont, Z., Lohmann, U., Schwarz, J. P., Shindell, D., Storelvmo, T., Warren, S. G., and Zender, C. S.: Bounding the role of black carbon in the climate system: a scientific assessment, J. Geophys. Res.-Atmos., 118, 5380–5552, 2013.
Cappa, C. D., Che, D. L., Kessler, S. H., Kroll, J. H., and Wilson, K. R.: Variations in organic aerosol optical and hygroscopic properties upon heterogeneous OH oxidation, J. Geophys. Res.-Atmos., 116, D15204, doi:10.1029/2011jd015918, 2011.
Cappa, C. D., Onasch, T. B., Massoli, P., Worsnop, D. R., Bates, T. S., Cross, E. S., Davidovits, P., Hakala, J., Hayden, K. L., Jobson, B. T., Kolesar, K. R., Lack, D. A., Lerner, B. M., Li, S.-M., Mellon, D., Nuaaman, I., Olfert, J. S., Petäjä, T., Quinn, P. K., Song, C., Subramanian, R., Williams, E. J., and Zaveri, R. A.: Radiative absorption enhancements due to the mixing state of atmospheric black carbon, Science, 337, 1078–1081, 2012.
Chen, Y. and Bond, T. C.: Light absorption by organic carbon from wood combustion, Atmos. Chem. Phys., 10, 1773–1787, doi:10.5194/acp-10-1773-2010, 2010.





ACPD
14, 4149–4187, 2014



Chung, C. E., Ramanathan, V., and Decremer, D.: Observationally constrained estimates of carbonaceous aerosol radiative forcing, P. Natl. Acad. Sci. USA, 109, 11624–11629, 2012.
Daumit, K. E., Kessler, S. H., and Kroll, J. H.: Average chemical properties and potential formation pathways of highly oxidized organic aerosol, Faraday Discuss., 165, 181–202, 2013.
DeCarlo, P. F., Slowik, J. G., Worsnop, D. R., Davidovits, P., and Jimenez, J. L.: Particle morphology and density characterization by combined mobility and aerodynamic diameter measurements – Part 1: Theory, Aerosol Sci. Tech., 38, 1185–1205, doi:10.1080/027868290903907, 2004.
DeCarlo, P. F., Kimmel, J. R., Trimborn, A., Northway, M. J., Jayne, J. T., Aiken, A. C., Gonin, M., Fuhrer, K., Horvath, T., Docherty, K. S., Worsnop, D. R., and Jimenez, J. L.: Field-deployable, high-resolution, time-of-flight aerosol mass spectrometer, Anal. Chem., 78, 8281–8289, 2006.
Emanuelsson, E. U., Hallquist, M., Kristensen, K., Glasius, M., Bohn, B., Fuchs, H., Kammer, B., Kiendler-Scharr, A., Nehr, S., Rubach, F., Tillmann, R., Wahner, A., Wu, H.-C., and Mentel, Th. F.: Formation of anthropogenic secondary organic aerosol (SOA) and its influence on biogenic SOA properties, Atmos. Chem. Phys., 13, 2837–2855, doi:10.5194/acp-13-2837-2013, 2013a.
Emanuelsson, E. U., Watne, Å. K., Lutz, A., Ljungström, E., and Hallquist, M.: Influence of humidity, temperature, and radicals on the formation and thermal properties of Secondary Organic Aerosol (SOA) from ozonolysis of $\beta$-pinene, J. Phys. Chem. A, 117, 10346–10358, 2013b.
Feng, Y., Ramanathan, V., and Kotamarthi, V. R.: Brown carbon: a significant atmospheric absorber of solar radiation?, Atmos. Chem. Phys., 13, 8607–8621, doi:10.5194/acp-13-8607-2013, 2013.
Fuchs, H., Dorn, H.-P., Bachner, M., Bohn, B., Brauers, T., Gomm, S., Hofzumahaus, A., Holland, F., Nehr, S., Rohrer, F., Tillmann, R., and Wahner, A.: Comparison of OH concentration measurements by DOAS and LIF during SAPHIR chamber experiments at high OH reactivity and low NO concentration, Atmos. Meas. Tech., 5, 1611–1626, doi:10.5194/amt-5-1611-2012, 2012.
Glasius, M., la Cour, A., and Lohse, C.: Fossil and nonfossil carbon in fine particulate matter: a study of five European cities, J. Geophys. Res.-Atmos., 116, D11302, doi:10.1029/2011jd015646, 2011.





ACPD
14, 4149–4187, 2014



Hallquist, M., Wenger, J. C., Baltensperger, U., Rudich, Y., Simpson, D., Claeys, M., Dommen, J., Donahue, N. M., George, C., Goldstein, A. H., Hamilton, J. F., Herrmann, H., Hoffmann, T., Iinuma, Y., Jang, M., Jenkin, M. E., Jimenez, J. L., Kiendler-Scharr, A., Maenhaut, W., McFiggans, G., Mentel, Th. F., Monod, A., Prévôt, A. S. H., Seinfeld, J. H., Surratt, J. D., Szmigielski, R., and Wildt, J.: The formation, properties and impact of secondary organic aerosol: current and emerging issues, Atmos. Chem. Phys., 9, 5155–5236, doi:10.5194/acp-9-5155-2009, 2009.

Hildebrandt, L., Henry, K. M., Kroll, J. H., Worsnop, D. R., Pandis, S. N., and Donahue, N. M.: Evaluating the mixing of organic aerosol components using high-resolution aerosol mass spectrometry, Environ. Sci. Technol., 45, 6329–6335, 2011.

Hoyle, C. R., Boy, M., Donahue, N. M., Fry, J. L., Glasius, M., Guenther, A., Hallar, A. G., Huff Hartz, K., Petters, M. D., Petäjä, T., Rosenoern, T., and Sullivan, A. P.: A review of the anthropogenic influence on biogenic secondary organic aerosol, Atmos. Chem. Phys., 11, 321–343, doi:10.5194/acp-11-321-2011, 2011.

Jonsson, Å. M., Hallquist, M., and Saathoff, H.: Volatility of secondary organic aerosols from the ozone initiated oxidation of -pinene and limonene, J. Aerosol Sci., 38, 843–852, 2007.

Jordan, A., Haidacher, S., Hanel, G., Hartungen, E., Märk, L., Seehauser, H., Schottkowsky, R., Sulzer, P., and Märk, T. D.: A high resolution and high sensitivity proton-transfer-reaction time-of-flight mass spectrometer (PTR-TOF-MS), Int. J. Mass Spectrom., 286, 122–128, 2009.

Katrib, Y., Martin, S. T., Rudich, Y., Davidovits, P., Jayne, J. T., and Worsnop, D. R.: Density changes of aerosol particles as a result of chemical reaction, Atmos. Chem. Phys., 5, 275–291, doi:10.5194/acp-5-275-2005, 2005.

Kautzman, K. E., Surratt, J. D., Chan, M. N., Chan, A. W. H., Hersey, S. P., Chhabra, P. S., Dalleska, N. F., Wennberg, P. O., Flagan, R. C., and Seinfeld, J. H.: Chemical composition of gas- and aerosol-phase products from the photooxidation of naphthalene, J. Phys. Chem. A, 114, 913–934, 2010.

Kim, H. and Paulson, S. E.: Real refractive indices and volatility of secondary organic aerosol generated from photooxidation and ozonolysis of limonene, $\alpha$-pinene and toluene, Atmos. Chem. Phys., 13, 7711–7723, doi:10.5194/acp-13-7711-2013, 2013.

Kim, H., Barkey, B., and Paulson, S. E.: Real refractive indices of $\alpha$- and $\beta$-pinene and toluene secondary organic aerosols generated from ozonolysis and photo-oxidation, J. Geophys. Res.-Atmos., 115, D24212, doi:10.1029/2010jd014549, 2010.





ACPD
14, 4149–4187, 2014



Kim, H., Barkey, B., and Paulson, S. E.: Real refractive indices and formation yields of secondary organic aerosol generated from photooxidation of limonene and $\alpha$-pinene: the effect of the HC/$NO_x$ ratio, J. Phys. Chem. A, 116, 6059–6067, 2012.

Kirchstetter, T. W. and Thatcher, T. L.: Contribution of organic carbon to wood smoke particulate matter absorption of solar radiation, Atmos. Chem. Phys., 12, 6067–6072, doi:10.5194/acp-12-6067-2012, 2012.

Koren, I., Martins, J. V., Remer, L. A., and Afargan, H.: Smoke invigoration versus inhibition of clouds over the Amazon, Science, 321, 946–949, doi:10.1126/science.1159185, 2008.

Lack, D. A., Lovejoy, E. R., Baynard, T., Pettersson, A., and Ravishankara, A. R.: Aerosol absorption measurement using photoacoustic spectroscopy: sensitivity, calibration, and uncertainty developments, Aerosol Sci. Tech., 40, 697–708, 2006.

Lambe, A. T., Cappa, C. D., Massoli, P., Onasch, T. B., Forestieri, S. D., Martin, A. T., Cummings, M. J., Croasdale, D. R., Brune, W. H., Worsnop, D. R., and Davidovits, P.: Relationship between oxidation level and optical properties of secondary organic aerosol, Environ. Sci. Technol., 47, 6349–6357, 2013.

Lang-Yona, N., Rudich, Y., Segre, E., Dinar, E., and Abo-Riziq, A.: Complex refractive indices of aerosols retrieved by continuous wave-cavity ring down aerosol spectrometer, Anal. Chem., 81, 1762–1769, 2009.

Lang-Yona, N., Rudich, Y., Mentel, Th. F., Bohne, A., Buchholz, A., Kiendler-Scharr, A., Kleist, E., Spindler, C., Tillmann, R., and Wildt, J.: The chemical and microphysical properties of secondary organic aerosols from Holm Oak emissions, Atmos. Chem. Phys., 10, 7253–7265, doi:10.5194/acp-10-7253-2010, 2010.

Liu, Y. and Daum, P. H.: Relationship of refractive index to mass density and self-consistency of mixing rules for multicomponent mixtures like ambient aerosols, J. Aerosol Sci., 39, 974–986, 2008.

Liu, P., Zhang, Y., and Martin, S. T.: Complex refractive indices of thin films of secondary organic materials by spectroscopic ellipsometry from 220 to 1200 nm, Environ. Sci. Technol., 47, 13594–13601, 2013.

Michel Flores, J., Bar-Or, R. Z., Bluvshtein, N., Abo-Riziq, A., Kostinski, A., Borrmann, S., Koren, I., Koren, I., and Rudich, Y.: Absorbing aerosols at high relative humidity: linking hygroscopic growth to optical properties, Atmos. Chem. Phys., 12, 5511–5521, doi:10.5194/acp-12-5511-2012, 2012.





ACPD
14, 4149–4187, 2014



Miles, R. E. H., Rudic, S., Orr-Ewing, A. J., and Reid, J. P.: Measurements of the wavelength dependent extinction of aerosols by cavity ring down spectroscopy, Phys. Chem. Chem. Phys., 12, 3914–3920, 2010.

Nakayama, T., Matsumi, Y., Sato, K., Imamura, T., Yamazaki, A., and Uchiyama, A.: Laboratory studies on optical properties of secondary organic aerosols generated during the photooxidation of toluene and the ozonolysis of $\alpha$-pinene, J. Geophys. Res.-Atmos., 115, D24204, doi:10.1029/2010jd014387, 2010.

Nakayama, T., Sato, K., Matsumi, Y., Imamura, T., Yamazaki, A., and Uchiyama, A.: Wavelength dependence of refractive index of secondary organic aerosols generated during the ozonolysis and photooxidation of $\alpha$-pinene, Sola, 8, 119–123, 2012.

Nakayama, T., Sato, K., Matsumi, Y., Imamura, T., Yamazaki, A., and Uchiyama, A.: Wavelength and $NO_x$ dependent complex refractive index of SOAs generated from the photooxidation of toluene, Atmos. Chem. Phys., 13, 531–545, doi:10.5194/acp-13-531-2013, 2013.

Ng, N. L., Canagaratna, M. R., Zhang, Q., Jimenez, J. L., Tian, J., Ulbrich, I. M., Kroll, J. H., Docherty, K. S., Chhabra, P. S., Bahreini, R., Murphy, S. M., Seinfeld, J. H., Hildebrandt, L., Donahue, N. M., DeCarlo, P. F., Lanz, V. A., Prévôt, A. S. H., Dinar, E., Rudich, Y., and Worsnop, D. R.: Organic aerosol components observed in Northern Hemispheric datasets from Aerosol Mass Spectrometry, Atmos. Chem. Phys., 10, 4625–4641, doi:10.5194/acp-10-4625-2010, 2010.

Ofner, J., Krüger, H.-U., Grothe, H., Schmitt-Kopplin, P., Whitmore, K., and Zetzsch, C.: Physicochemical characterization of SOA derived from catechol and guaiacol – a model substance for the aromatic fraction of atmospheric HULIS, Atmos. Chem. Phys., 11, 1–15, doi:10.5194/acp-11-1-2011, 2011.

Park, R. J., Kim, M. J., Jeong, J. I., Youn, D., and Kim, S.: A contribution of brown carbon aerosol to the aerosol light absorption and its radiative forcing in East Asia, Atmos. Environ., 44, 1414–1421, 2010.

Pettersson, A., Lovejoy, E. R., Brock, C. A., Brown, S. S., and Ravishankara, A. R.: Measurement of aerosol optical extinction at 532 nm with pulsed cavity ring down spectroscopy, J. Aerosol Sci., 35, 995–1011, doi:10.1016/j.jaerosci.2004.02.008, 2004.

Redmond, H. and Thompson, J. E.: Evaluation of a quantitative structure–property relationship (QSPR) for predicting mid-visible refractive index of secondary organic aerosol (SOA), Phys. Chem. Chem. Phys., 13, 6872–6882, 2011.





ACPD
14, 4149–4187, 2014



Rohrer, F., Bohn, B., Brauers, T., Brüning, D., Johnen, F.-J., Wahner, A., and Kleffmann, J.: Characterisation of the photolytic HONO-source in the atmosphere simulation chamber SAPHIR, Atmos. Chem. Phys., 5, 2189–2201, doi:10.5194/acp-5-2189-2005, 2005.

Salo, K., Hallquist, M., Jonsson, Å. M., Saathoff, H., Naumann, K.-H., Spindler, C., Tillmann, R., Fuchs, H., Bohn, B., Rubach, F., Mentel, Th. F., Müller, L., Reinnig, M., Hoffmann, T., and Donahue, N. M.: Volatility of secondary organic aerosol during OH radical induced ageing, Atmos. Chem. Phys., 11, 11055–11067, doi:10.5194/acp-11-11055-2011, 2011.

Schnaiter, M., Horvath, H., Möhler, O., Naumann, K. H., Saathoff, H., and Schöck, O. W.: UV-VIS-NIR spectral optical properties of soot and soot-containing aerosols, J. Aerosol Sci., 34, 1421–1444, 2003.

Shilling, J. E., Chen, Q., King, S. M., Rosenoern, T., Kroll, J. H., Worsnop, D. R., DeCarlo, P. F., Aiken, A. C., Sueper, D., Jimenez, J. L., and Martin, S. T.: Loading-dependent elemental composition of $\alpha$-pinene SOA particles, Atmos. Chem. Phys., 9, 771–782, doi:10.5194/acp-9-771-2009, 2009.

Spracklen, D. V., Jimenez, J. L., Carslaw, K. S., Worsnop, D. R., Evans, M. J., Mann, G. W., Zhang, Q., Canagaratna, M. R., Allan, J., Coe, H., McFiggans, G., Rap, A., and Forster, P.: Aerosol mass spectrometer constraint on the global secondary organic aerosol budget, Atmos. Chem. Phys., 11, 12109–12136, doi:10.5194/acp-11-12109-2011, 2011.

van Krevelen, D.: Graphical-statistical method for the study of structure and reaction processes of coal, Fuel, 24, 269–284, 1950.

Walser, M. L., Desyaterik, Y., Laskin, J., Laskin, A., and Nizkorodov, S. A.: High-resolution mass spectrometric analysis of secondary organic aerosol produced by ozonation of limonene, Phys. Chem. Chem. Phys., 10, 1009–1022, 2008.

Washenfelder, R. A., Flores, J. M., Brock, C. A., Brown, S. S., and Rudich, Y.: Broadband measurements of aerosol extinction in the ultraviolet spectral region, Atmos. Meas. Tech., 6, 861–877, doi:10.5194/amt-6-861-2013, 2013.

Wex, H., Petters, M. D., Carrico, C. M., Hallbauer, E., Massling, A., McMeeking, G. R., Poulain, L., Wu, Z., Kreidenweis, S. M., and Stratmann, F.: Towards closing the gap between hygroscopic growth and activation for secondary organic aerosol: Part 1 – Evidence from measurements, Atmos. Chem. Phys., 9, 3987–3997, doi:10.5194/acp-9-3987-2009, 2009.

Wiedensohler, A.: An approximation of the bipolar charge distribution for particles in the submicron size range, J. Aerosol Sci., 19, 387–389, 1988.





ACPD
14, 4149–4187, 2014



Yu, Y., Ezell, M. J., Zelenyuk, A., Imre, D., Alexander, L., Ortega, J., D'Anna, B., Harmon, C. W., Johnson, S. N., and Finlayson-Pitts, B. J.: Photooxidation of $\alpha$-pinene at high relative humidity in the presence of increasing concentrations of $NO_x$, Atmos. Environ., 42, 5044–5060, 2008.

Zhao, W., Dong, M., Chen, W., Gu, X., Hu, C., Gao, X., Huang, W., and Zhang, W.: Wavelength-resolved optical extinction measurements of aerosols using broad-band cavity-enhanced absorption spectroscopy over the spectral range of 445–480 nm, Anal. Chem., 85, 2260–2268, 2013.





ACPD
14, 4149–4187, 2014



**Table 1.** Description of the experiments performed in this study.

| Experiment | Description | VOC (ppb) | Initial [OH] ($\times 10^6$ molec cm$^{-3}$) | [$NO_x$] (ppbv) | Total duration |
|---|---|---|---|---|---|
| BVOCs | BVOCs mix only | $\alpha$-pinene, limonene (48, 48) | 7.4 | < 0.25 | ~ 50 h. |
| Sequential | BVOCs mix and p-xylene-$d_{10}$ (p-xylene-$d_{10}$ added 5 h after BVOCs mix) | $\alpha$-pinene, limonene (39, 39) p-xylene-$d_{10}$ (51) | 7.8 | < 0.30 | ~ 29 h. |
| Mixture | BVOCs mix and p-xylene-$d_{10}$ (added together) | $\alpha$-pinene, limonene (42, 42) p-xylene-$d_{10}$ (90) | 8.0 | < 0.25 | ~ 29.5 h. |





ACPD
14, 4149–4187, 2014



**Table 2.** Real parts of the RI for different O/C ratios in this study compared with literature values.

| Real part ($n$) of the RI | O/C atomic ratio | VOC | SOA formation | Wavelength (nm) | Reference |
|---|---|---|---|---|---|
| 1.502 (±0.004)–1.493 (±0.004) | 0.37–0.38 | $\alpha$-pinene + limonene | ozonolysis and OH oxidation | 405 | This work |
| 1.460 (±0.003)–1.504 (±0.020) | 0.39–0.44 | $\alpha$-pinene + limonene + p-xylene-$d_{10}$ (added 5 h after) | ozonolysis and OH oxidation | 405 | This work |
| 1.462 (±0.005)–1.513 (±0.009) | 0.35–0.42 | $\alpha$-pinene + limonene + p-xylene-$d_{10}$ | ozonolysis and OH oxidation | 405 | This work |
| 1.511 (±0.003) | < 0.3 | $\alpha$-pinene | ozonolysis | 405 | Liu et al. (2013) |
| 1.514 (±0.003) | < 0.3 | limonene | ozonolysis | 405 | Liu et al. (2013) |
| 1.51 (±0.02)–1.45 (±0.04) | 0.42–0.93 | $\alpha$-pinene | OH oxidation | 405 | Lambe et al. (2013) |
| 1.66 (±0.04)–1.58 (±0.06) | 0.52–1.29 | naphthalene | OH oxidation | 405 | Lambe et al. (2013) |
| 1.55 (±0.01)–1.53 (±0.01) | 0.70–1.14 | guaiacol | OH oxidation | 405 | Lambe et al. (2013) |
| 1.54 (±0.01)–1.48 (±0.01) | 0.37–0.89 | tricycle[5.2.$1.0^{2,6}$]decane | OH oxidation | 405 | Lambe et al. (2013) |
| 1.449 (±0.030)–1.567 (±0.043) | 0.64–0.73 | toluene | photooxidation | 405 | Nakayama et al. (2013) |
| 1.431 (±0.026)–1.498 (±0.025) | 0.64–0.73 | toluene | photooxidation | 532 | Nakayama et al. (2013) |
| 1.475 (±0.022)–1.498 (±0.030) | 0.43–0.47 | $\alpha$-pinene | ozonolysis and photooxidation | 405 | Nakayama et al. (2012) |
| 1.476 (±0.021)–1.458 (±0.02) | 0.43–0.47 | $\alpha$-pinene | ozonolysis and photooxidation | 532 | Nakayama et al. (2012) |
| 1.47 (±0.02)–1.52 (±0.00) | 0–0.35 | squalene | OH oxidation | 532 | Cappa et al. (2011) |
| 1.47 (±0.02)–1.54 (±0.00) | 0.45–0.75 | azelaic acid | OH oxidation | 532 | Cappa et al. (2011) |





ACPD
14, 4149–4187, 2014



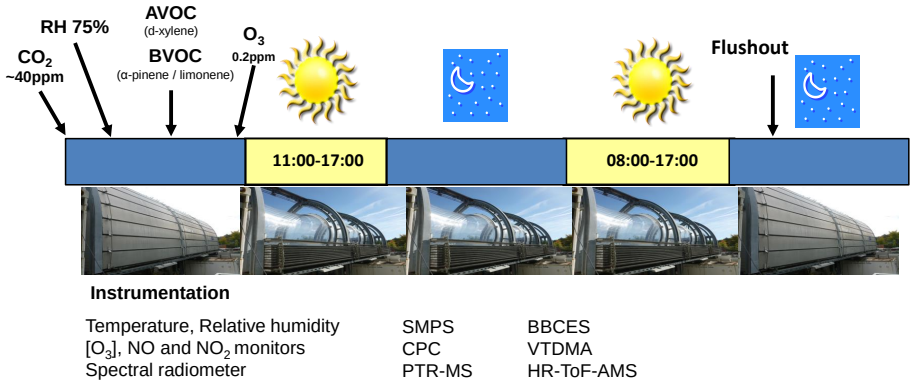


**Fig. 1.** Schematic of the experimental procedure and instrumentation used for measuring the evolution of secondary organic aerosol over a diurnal cycle.
Acronyms:
SMPS – Scanning mobility particle sizer;
CPC – condensation particle counter;
PTR-MS – proton transfer reaction-mass spectrometer;
BBCES – Broadband cavity enhanced spectrometer;
VTDMA – volatility tandem differential mobility analyser;
HR-ToF-AMS – high resolution-time of flight-aerosol mass spectrometer.





ACPD
14, 4149–4187, 2014



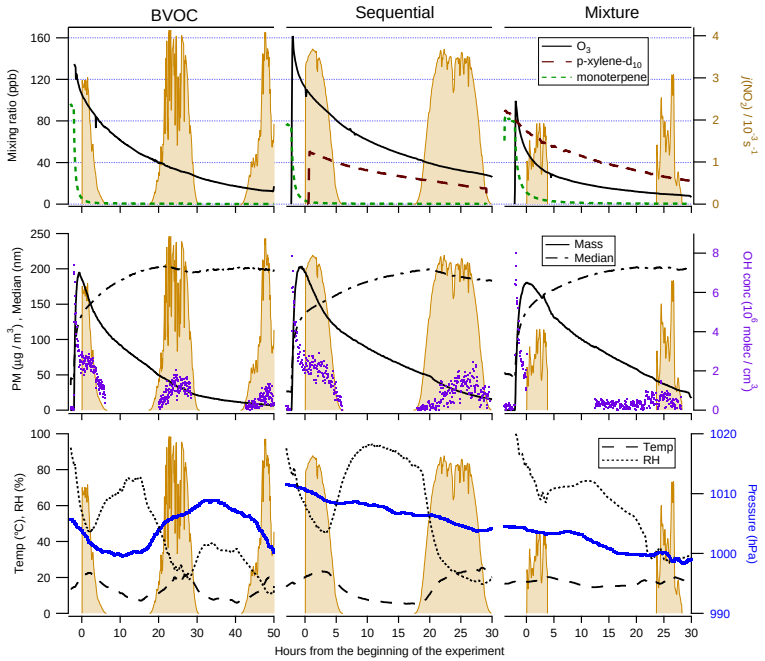


**Fig. 2.** Van Krevelen diagram showing the ratio of H / C to O / C measured for the three experiments performed in this study: a mixture of $\alpha$-pinene with limonene (green diamons), a mixture of $\alpha$-pinene with limonene with a sequential addition of p-xylene-$d_{10}$ (grey squares), and a mixture of $\alpha$-pinene, limonene and p-xylene-d10 (orange circles). The change in marker size depicts time; smaller markers refer to the beginning of the experiment, and larger markers to the end. **(A)** shows specifically the three experiments performed in this study. The darker colours depict night time. in **(B)**, the results are compared to the low volatility oxygenated organic aerosol factors from HR-AMS field campaigns (numbered circles, adapted from Daumit et al. (2013)), results for $\alpha$-pinene SOA from Lambe et al. (2013) (red triangles), and Nakayama et al. (2012) (blue inverted triangles), and squalene SOA from Cappa et al. (2011) (black rhombus).





ACPD
14, 4149–4187, 2014



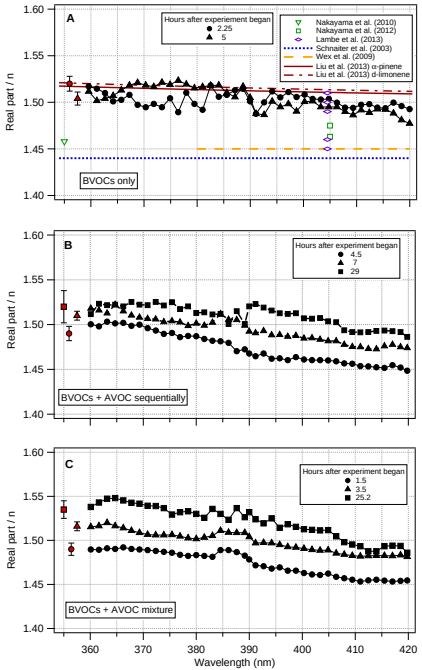


**Fig. 3.** Change of the real part of the complex refractive index vs. wavelength as a function of time for SOA produced from **(A)** only a mixture of $\alpha$-pinene and limonene, compared to literature values of the real RI of $\alpha$-pinene; **(B)** a mixture of $\alpha$-pinene and limonene followed by the addition of p-xylene-$d_{10}$ 5 h after, and **(C)** a mixture of $\alpha$-pinene, limonene and p-xylene-$d_{10}$ (only 3 retrievals are shown for clarity). The averaged error bars of the retrieved RI values are shown as the red markers on the left for clarity. The average errors for the retrievals in **(A)** are: 0.008 (±0.008), and 0.006 (±0.005) for 2.25 h and 5 h, respectively. The average errors for the retrievals in **(B)** are: 0.005 (±0.008), 0.004 (±0.001), and 0.018 (±0.007) for 4.5 h, 7 h, and 29 h, respectively. The average errors for the retrievals in **(C)** are: 0.007 (± 0.006), 0.004 (± 0.003), and 0.010 (± 0.004) for 1.5 h, 7 h, and 25.2 h, respectively.





ACPD
14, 4149–4187, 2014



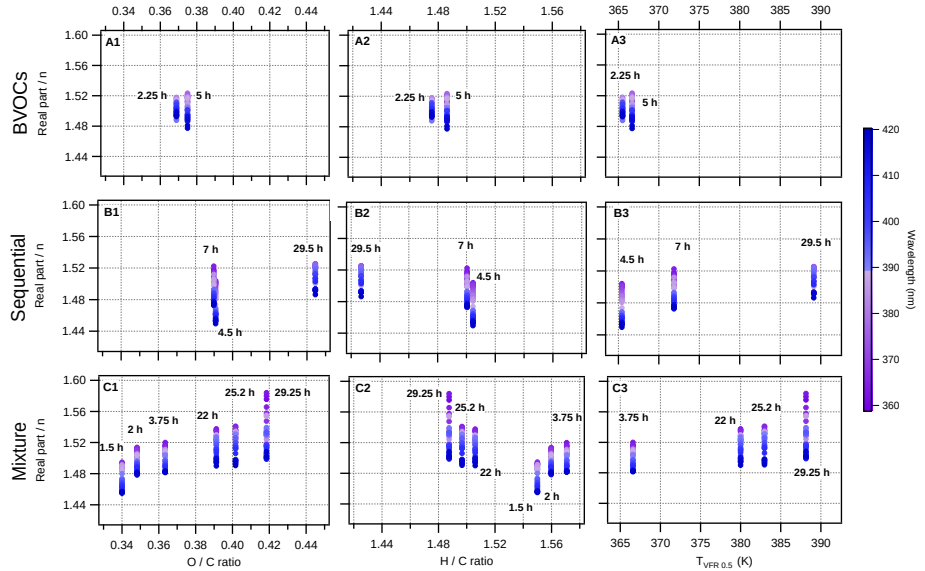


**Fig. 4.** The change in time (given in hours, shown next to the retrieved values) for the retrieved real part of the RI as a function of O/C ratio (panels A1, B1 and C1), H/C ratio (panels A2, B2 and C2), and $T_{VFR0.5}$ (the temperature at which the volume fraction remaining was reduced by half, panels A3, B3 and C3). The top panels – A1, A2 and A3 – show the results for the SOA produced from a 1 to 1 mixture of $\alpha$-pinene and limonene. The middle panels – B1, B2, and B3 – show the results for the SOA produced from the mixture of $\alpha$-pinene, limonene, and p-xylene-$d_{10}$. The lower panels – C1, C2, and C3 – show the results for the SOA produced from the sequential addition of the mixture of $\alpha$-pinene and limonene followed by p-xylene-$d_{10}$. The color scale indicates the measured wavelength. The error bars for the O/C (31 %), H/C (10 %), and $T_{VFR0.5}$ are not shown for clarity. The average error for the $T_{VFR0.5}$ is 2.3 K.





ACPD
14, 4149–4187, 2014



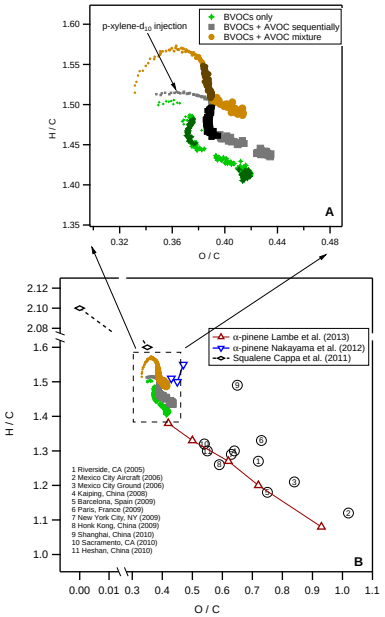


**Fig. 5.** Van Krevelen diagram showing the ratio of H/C to O/C measured for the three experiments performed in this study: a mixture of $\alpha$-pinene with limonene (green diamons), a mixture of $\alpha$-pinene with limonene with a sequential addition of p-xylene-$d_{10}$ (grey squares), and a mixture of $\alpha$-pinene, limonene and p-xylene-$d_{10}$ (orange circles). The change in marker size depicts time; smaller markers refer to the beginning of the experiment, and larger markers to the end. The top panel **(A)** shows specifically the three experiments performed in this study. The darker colours depict night time. In the lower panel **(B)**, the results are compared to the low volatility oxygenated organic aerosol factors from HR-AMS field campaigns (numbered circles, adapted from Daumit et al., 2013), results for $\alpha$-pinene SOA from Lambe et al. (2013) (red triangles), and Nakayama et al. (2012) (blue inverted triangles), and squalene SOA from Cappa et al. (2011) (black rhombus).





ACPD
14, 4149–4187, 2014



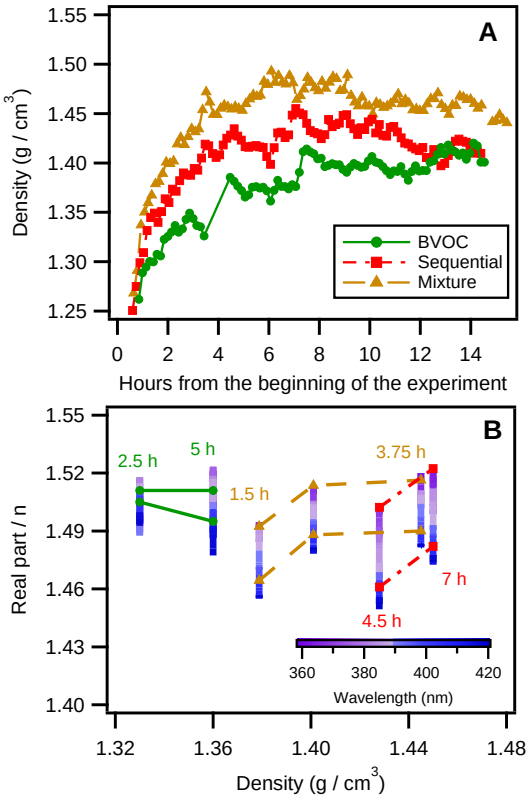


**Fig. 6. (A)** Time series of the density measured for the BVOC (green circles), the sequential (red squares); and the mixture (orange triangles) experiment. **(B)** The change in time of the real part of the RI vs. density for each experiment performed. The colour bars show the span in the RI for the wavelengths measured, the time span between the measurements is written above (for the BVOC and sequential experiments) and below (the mixture experiment) each set of measurements.





ACPD
14, 4149–4187, 2014



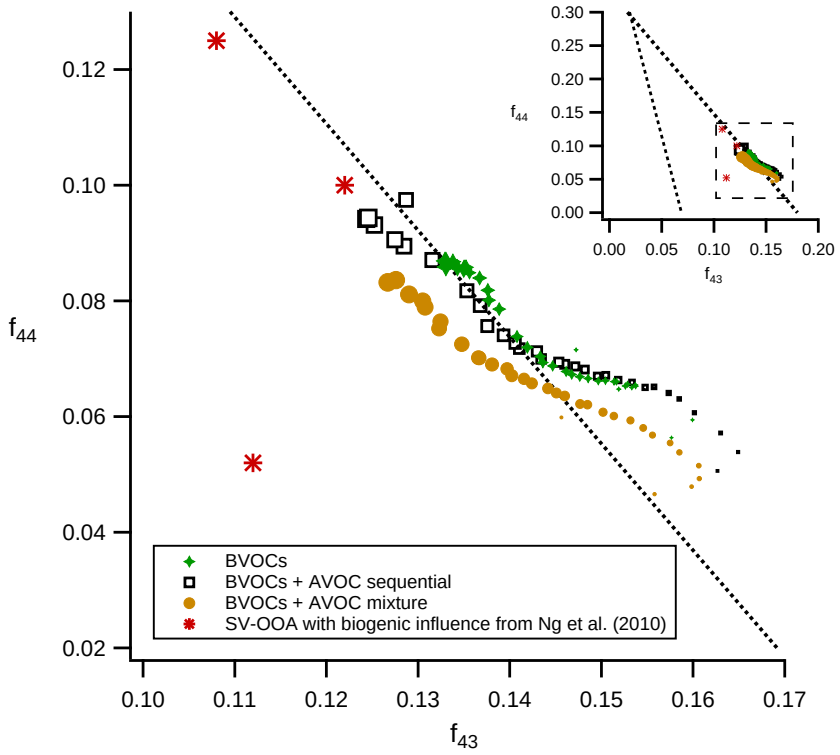


**Fig. 7.** $f_{44}$ vs. $f_{43}$ for the SOA produced from the mixture of $\alpha$-pinene and limonene (green diamonds), from the sequential addition of the mixture of $\alpha$-pinene and limonene followed by p-xylene-$d_{10}$ (black squares), and from the mixture of $\alpha$-pinene, limonene, and p-xylene-$d_{10}$ (orange circles). The change in size of the markers depicts time; smaller markers refer to the beginning of the experiment, and larger markers to the end. The insert shows the total triangular area (dotted lines) that represents the common values of ambient oxygenated organic aerosol components, adapted from Ng et al. (2010).





ACPD
14, 4149–4187, 2014



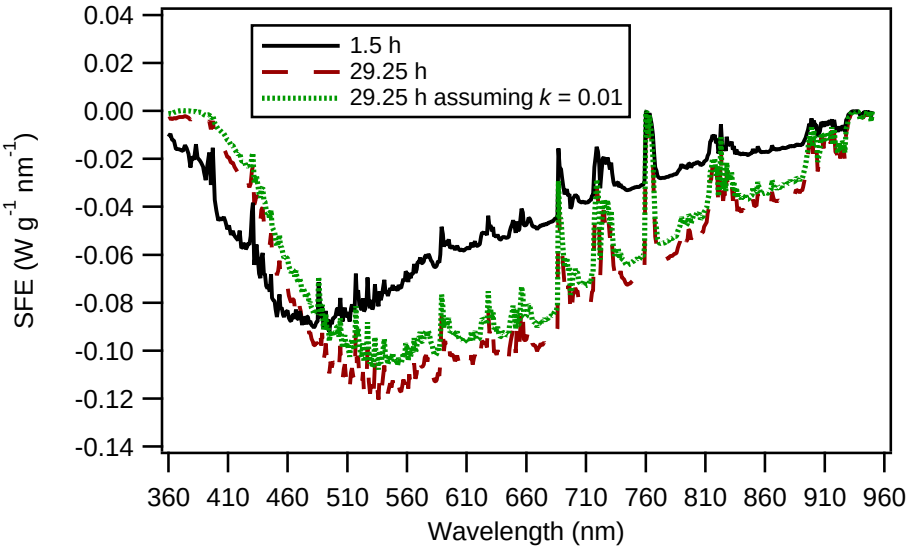


**Fig. 8.** Simple forcing efficiency calculated using the first (black line) and last (red dashed line) retrieved RI values from the mixture experiment. The green dotted line represents a scenario in which the imaginary part of the last retrieval increased to $k = 0.01$.





ACPD
14, 4149–4187, 2014